Brodogradnja Volume 77 Number 1 (2026) 77106

journal homepage: www.brodogradnja.fsb.hr

Brodogradnja

An International Journal of Naval Architecture and Ocean Engineering for Research and Development

Determination of the safety exclusion zone for battery-powered ship with consideration of fire accident

Wenfen Zhang[1,2,3], *Yunling Zhang*[1], *Bing Wu*[2,*], *Yang Yu*[2], *Yupeng Yuan*[2]

[1] *School of Management, Wuhan Textile University, Wuhan 430073, China*
[2] *State Key Laboratory of Maritime Technology and Safety, National Engineering Research Center for water Transport safety, Wuhan University of Technology, Wuhan 430063, China*
[3] *Enterprise Decision Support Research Center, The Hubei Key Research Base of Humanities and Social Sciences, Wuhan 430073, China*

ARTICLE INFO

Keywords:
Safety exclusion zone
Battery-powered ship
Fire accident
Thermal radiation

ABSTRACT

Battery-powered ships have been developed quickly owing to the international dual carbon strategy and net-zero initiatives. However, the safety of battery-powered ships has attracted much attention because of the high frequency of fire accidents, and maintaining a safety distance between a battery-powered ship and nearby vessels is a proven method to mitigate risks. The large battery capacity poses significant challenges due to intense thermal radiation during fires. Thus, this paper proposes a novel method for determining the safety exclusion zone to mitigate the consequences of collision accidents while considering the thermal runaway of the battery. On basis of a thermal radiation model, the safety distance for avoiding radiation damage is determined by setting the acceptable thermal radiation flux as the threshold level. Afterward, a ship domain model and following theory are used to calculate the longitudinal and lateral safety distances of a battery-powered ship. Finally, a computational fluid dynamics simulation-based case study is carried out to demonstrate the application of the proposed method. This study provides critical insights for policymakers and researchers in advancing maritime safety protocols.

1. Introduction

As electrification is viewed as a crucial pathway toward decarbonization for maritime transportation, battery-powered ships have been developed quickly in recent years. According to the latest Clarkson Research report, 715 battery-powered vessels were in active service globally as of June 2025, with an additional 504 units on order. New vessel orders surged by 72.5 % year-on-year during the first half of 2025. By 2030, the global market for battery-powered ships is expected to exceed 10.5 billion dollars. Batteries effectively integrate renewable energy and enable ships to shift from traditional fuels to clean energy [1-3]. This will drive their widespread use in hybrid vessels within the next decade [4].

In recent years, the safety of battery-powered ships has attracted much attention because of the high frequency of fire and explosion accidents. On October 10, 2019, the fire accident of MF Ytteroyningen, a

* Corresponding author.
E-mail address: bing.wu@whut.edu.cn

https://doi.org/10.21278/brod77106
Received 28 May 2025; Received in revised form 19 August 2025; Accepted 01 September 2025
Available online 12 September 2025
ISSN 0007-215X; eISSN 1845-5859

Norled-operated passenger vessel, caused 12 injuries due to toxic gas exposure during battery combustion. On March 11, 2021, the battery-powered catamaran MS Brim suffered a fire incident while docked in Norway's Oslofjord. Thermal runaway in Lithium-Ion Batteries (LIBs) generated explosive gases. On August 5, 2024, a battery-powered catamaran named Steady AF caught fire while docked at Longboat Key Marina in the USA, resulting in partial sinking of the vessel. There were nine incidents of battery-powered ship fires in China throughout 2024 according to media reports. This number has continued to increase in recent years.

Battery-powered ship fire poses severe threats to the safety of crew members and passengers. LIB fires release high-intensity thermal radiation, causing immediate casualties and igniting surrounding objects, thereby impeding evacuation and rescue operations [5]. Simultaneously, such fires generate thick smoke and toxic gases, resulting in respiratory failure or lethal intoxication. To mitigate these risks, current research focuses on improving emergency response capabilities through advanced firefighting systems designed for marine applications and real-time battery monitoring networks detecting thermal runaway [6].

Owing to potential battery explosions and flammable gas emissions, battery-powered ships have not been widely accepted by ship companies. To mitigate fire accidents that involve battery-powered ships, many studies have been carried out on the thermal runway and risk management of LIB failure [7], especially with respect to fire accident mechanisms, hazard identification, and ship battery fire consequences [8-11]. The disaster-causing mechanism and causal factors have been investigated, and the result have indicated that the State of Charge (SOC) is an important factor affecting the Thermal Runaway (TR) [10]. On basis of battery combustion characteristics, TR behaviour that results from the combustion of ship batteries with different SOCs has been identified [8, 9]. For fire risk hazard control, innovative approaches have been developed, including advanced materials, enhanced battery thermal management systems, and fault diagnosis technologies [12-14]. Battery-powered ships are equipped with large-scale battery systems, and several studies have been carried out on thermal management and fault diagnosis for such extensive battery configurations. Wu et al. [2] divided the Battery Thermal Management System (BTMS) into passive, active, and hybrid systems and examined how real-world working conditions, especially tilting, rolling, and vibration, affect BTMS. A data-driven method based on ship battery voltage has been proposed for fault diagnosis and detection, with the aim of predicting consistency faults during navigation [13]. Wang et al. [14] introduced an innovative flame-resistant composite phase transition material designed for battery thermal management in marine applications to mitigate thermal risks under extreme operational conditions.

However, the majority of the recent studies have focused on the safety of batteries from a micro perspective, while few studies intend to mitigate the consequence of collision accidents considering the thermal runaway of batteries. Despite advancements in technology and theory, the thermodynamic nature of lithium-based energy storage systems makes the complete elimination of fire risk impossible. Proximity to nearby vessels and personnel during a fire can trigger secondary disasters, which can have significant economic and safety impacts [15]. Maintaining safe distances in operational practice has been proven to be an effective measure for mitigating these consequences [16]. In view of size requirements for safety exclusion zones around incident vessels, it is imperative to establish appropriate safety exclusion zones specifically designed for battery-powered ships.

Research on safety exclusion zones has concentrated on traditional-fuel ships. A safety exclusion zone, which is an extension of the ship domain originally developed for collision avoidance, restricts access to unauthorized personnel and vessels. A systematic review of ship domain rules, guidelines, models and applications has been conducted [17-19]. Ship domain analysis has advanced through traditional structured methodologies: empirical analysis, expert systems, Multiple Criteria Decision Making (MCDM), and fuzzy logic. Moreover, technological advancements have driven extensive investigations into real-time modelling techniques, particularly intelligent solutions based on the Automatic Identification System (AIS) and Electronic Chart Display and Information System (ECDIS) [20-24]. Building upon the progress in ship domain research, studies have established maritime risk assessment frameworks for a variety of risk types, such as collision risks, potential risks, and grounding risks [25-27]. Notably, several studies have been conducted from a spatial perspective and have focused on specific waterborne domains, including ice-covered regions [28-30], open waters [31], busy ports [32], straits [33], inland waters [34] and coastal waters [21, 35].

Zarzycki et al. [36] utilized declarative methods to investigate ship domains and dynamic behaviour under favourable conditions.

Liquified Natural Gas (LNG) ships, which are a type of new energy ship, have garnered increasing attention concerning safety exclusion zones because of their major effects on waterway efficiency and operational safety [37]. Considering the fuel properties and dispersion dynamics of LNG, researchers have conducted extensive investigations into hazard-specific clearance distances with focused studies on leakage incidents and combustion scenarios [38-40]. Computational Fluid Dynamics (CFD) is widely used to simulate scenarios that involve leakage, combustion, and safety issues of ship alternative energy sources such as LNG and NH_3 [41-43]. Hazard impact ranges have been investigated by analysing diffusion characteristics, fire thermal radiation patterns, and population-independent parameters, to derive safety exclusion zones [44-46]. Various studies have integrated models such as the Solid Flame Model, Point Source Model, as well as deterministic approaches and risk-based approaches, to analyse hazard exclusion distances [47, 48].

Previous studies have lacked systematic research on safety exclusion zones for battery-powered ships. Recent research has focused on traditional diesel ships or LNG ships, with few studies specifically addressing the unique characteristics of battery-powered ships. The operational safety of battery-powered ships is inherently governed by their battery systems, with safety exclusion distances exhibiting three unique characteristics.

First, safety exclusion distances for battery-powered ships should be established to prevent both collisions and thermal radiation hazards during sailing in case of fire accident. Batteries are prone to fires and explosions during waterway transportation because of their high sensitivity to thermal instability, temperature fluctuations, complex navigation environment, overcharging, mechanical pressure, and impacts [2, 49, 50]. Second, the combustion mechanisms of battery fires differ fundamentally from those of traditional diesel or LNG fuels. These differences manifest in combustion parameter settings, spatiotemporal thermal radiation profiles, and hazard propagation to nearby ships and personnel. Third, factors that influence the thermal radiation distance in battery fires include the SOC and capacity scale of the battery. Battery capacity and SOC levels (e.g., 0 %, 50 % and 100 %) directly influence the mass loss rate and Heat Release Rate (HRR), thereby leading to distinct LIB combustion behaviours [51-53]. Very few studies devoted to research the thermal radiation of ship-powering batteries under various scenarios.

To address these issues, this study proposes a method for determining a battery-powered ship safety exclusion zone by integrating thermal radiation model and ship domain model, thereby providing insight into the appropriate level of the safety exclusion zone. This study investigates the effects of battery thermal radiation and collision avoidance for safe navigation and develops a method for determining the safety exclusion zone. The remainder of this paper is organized as follows. Section 2 proposes a safety exclusion zone framework for battery-powered ships based on a thermal radiation model, within which the core parameters critical to the framework's implementation are rigorously defined. In Section 3, a case study is conducted to demonstrate the application of the proposed methodology. Section 4 summarizes the main conclusions of the study.

2. Methodology: Safety exclusion zone based on Thermal Radiation Model

2.1 Framework of the proposed approach

In general, the safety exclusion zone refers to a restricted-access area where unauthorized entry is barred to reduce ignition risks and prevent personnel injuries. However, currently, the concept of safety exclusion zones for battery-powered ships has not been standardized or widely adopted. Referencing the concept of safety zones for LNG ships, this study develops a safety exclusion zone for battery-powered ships during fire incidents to prevent collisions and thermal radiation damage.

Specifically, the ship domain was initially proposed by Fuji (1971) [54] and is defined as a two-dimensional area that surrounds a ship for collision avoidance. Over the past four decades, numerous studies have developed distinct ship domain models characterized by varying geometric configurations (e.g., elliptical

and polygonal) and dimensional parameters, with these variations driven primarily by heterogeneous influencing factors.

Notably, the typical ship domain applies to traditional diesel-powered ships. Compared with traditional diesel-powered ship, the significant concern of battery-powered ship is the severity of the consequences caused by battery fire accidents. However, few studies have attempted to mitigate the consequences of collision accidents while considering the thermal runaway of batteries. The safety distance around a battery-powered ship should be large enough to avoid both collision and radiation damage. Therefore, the safety exclusion zone for a battery-powered ship is defined as the safety distance for collision avoidance plus the safety distance for radiation avoidance [55].

In Figure 1(I), the blue ship represents a traditional ship. Its surrounding blue ellipse defines the ship domain [17], which is quantified by two parameters: the longitudinal safety distance (a) and the lateral safety distance (b).

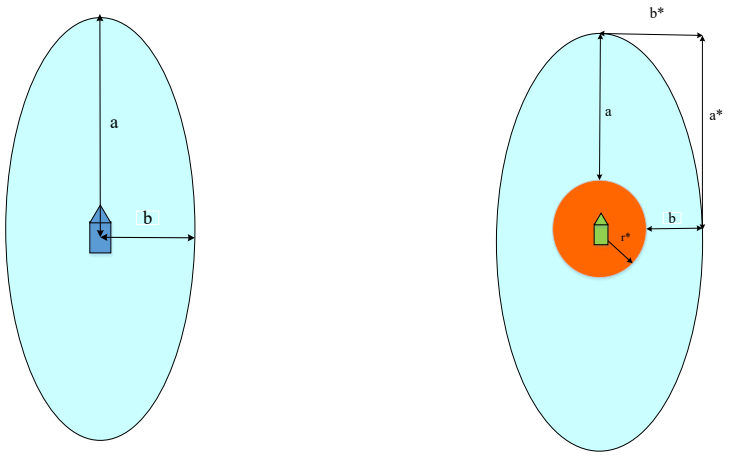

(I) Safety exclusion zone for a traditional ship (II) Safety exclusion zone for a battery-powered ship

Fig. 1. Safety exclusion zone for a traditional ship and a battery-powered ship

In Figure 1(II), the green ship is a battery-powered ship. The outer blue ellipse defines its safety exclusion zone, whereas the inner red circle represents the thermal radiation hazard area. The safety exclusion zone for a battery-powered ship can be quantified by two parameters: the longitudinal safety distance (a^*) and the lateral safety distance (b^*). The thermal radiation hazard area of the battery-powered ship has a radius r^*, where $a^* = a + r^*$, $b^* = b + r^*$.

Owing to the large scale of ship powering batteries, the thermal radiation to the surrounding area is very harmful [10]. This study aims to design appropriate safety exclusion zones to mitigate the consequences of collision accidents while considering the thermal runaway of batteries. This paper proposes a safety exclusion zone determination method aimed at mitigating the consequences of collision accidents while considering the thermal runaway of battery-powered ships. The framework is illustrated in Figure 2. The first step is to estimate the distance of radiation avoidance based on a thermal radiation model. Two classic thermal radiation models are introduced: the point source model and solid flame model. Based on the results of battery burning experiments, the parameter values involved in the thermal radiation models are obtained. Thermal radiation models are applied to study the thermal radiation distributions of battery cells burning under different SOC levels. By setting the acceptable thermal radiation flux for people and ship steel structure buildings as the threshold level, the acceptable safety distance for avoiding radiation damage is derived. Afterward, following theory and a classic ship domain model are applied to calculate the longitudinal and lateral safety distances for avoiding collisions. Finally, the safety exclusion zone of a battery-powered ship is determined through an integrated approach that combines the safety distance for thermal radiation avoidance with longitudinal and lateral collision-avoidance distances.

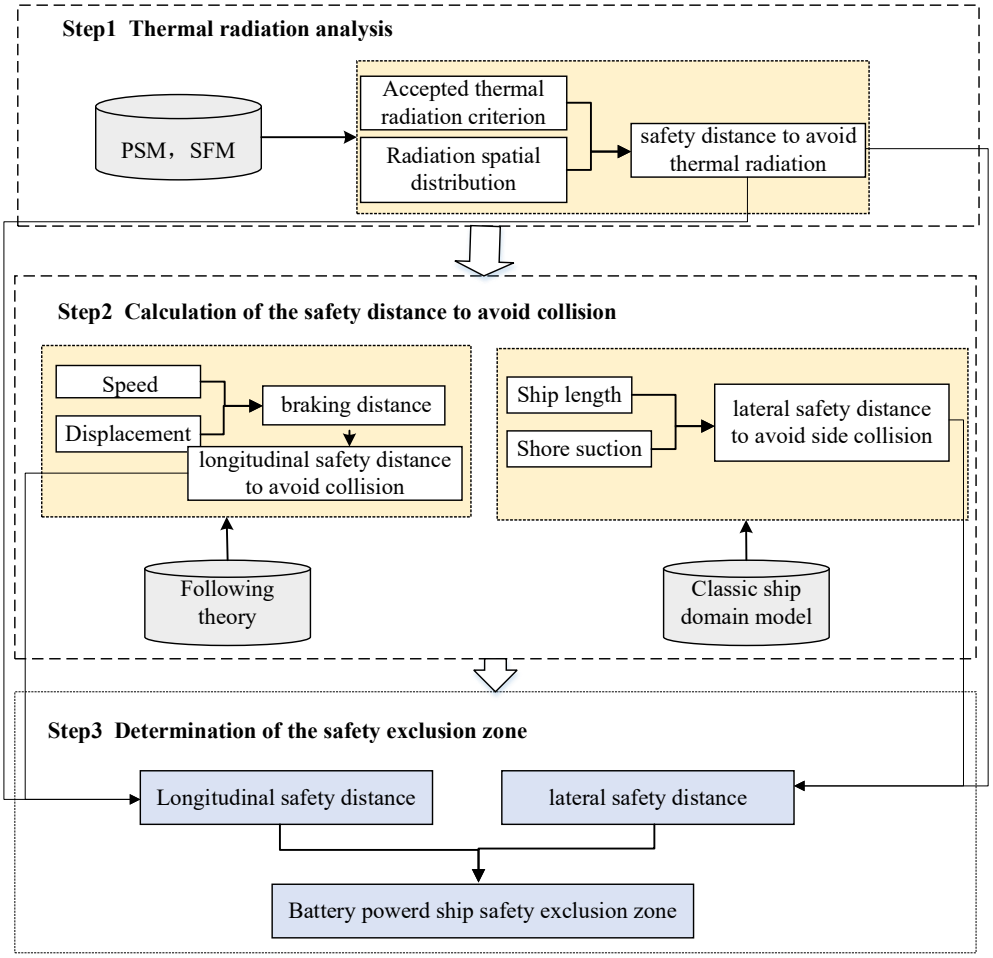

Fig. 2. Framework for determining the safety exclusion zone

2.2 Thermal radiation model

Thermal radiation to the surrounding area is a critical safety concern when a fire accident that involves battery-powered ship occurs. Compared with those of traditional diesel ships, the fire accident consequences of battery-powered ships are more serious owing to battery explosions and flammable gases. Several combustion parameters are measured, including the encompassing mass loss rate, time of ignition, HRR, flame temperature distribution [8, 56, 57]. Therefore, assessing the thermal radiation from battery-powered ships remains a key challenge that requires a thorough investigation. In this section, the spatial distribution of thermal radiation in the event of a battery fire is analysed to determine the safety distance for avoiding radiation damage. Two general approaches for thermal radiation modelling are the Point Source Model and the Solid Flame Model.

2.2.1 Point Source Model

The Point Source Model (PSM), which is widely employed in thermal radiation calculation, aims to estimate the heat release rate of fires. A hazardous radiant fraction of total energy releases and then spreads uniformly over the surface of a sphere whose radius is the distance from the fire centre to the exposed target, the PSM adheres to the inverse square law principle [58], which is expressed as Equation (1).

$$q''(s) = \chi_R \frac{Q}{4\pi s^2} \tag{1}$$

where s is the distance from fire centre to the exposed target (m), $q''(s)$ is the radiant heat flux (kW/m^2) received by the target located at distance s, χ_R is the fraction of combustion radiated energy, which is defined as 0.15~0.35 [58], $\chi_R = 0.2$, and Q is the heat release rate of the fire (kW).

2.2.2 Solid Flame Model

The Solid Flame Model (SFM) simplifies radiation analysis by approximating flames as geometrical cylinders. The equation of the SFM is expressed as the Equation (2) [47].

$$q''(s) = E \cdot F(s)\tau(s) \tag{2}$$

where E denotes the Mean Surface Emissive Power (MSEP), in kW/m^2, $F(s)$ represents the geometric view factor that quantifies the radiative fraction transferred from the flame centre to the target located at distance s, and $\tau(s)$ denotes the atmospheric transmissivity at a specified distance s.

MSEP over the entire flame surface is defined in Equation (3).

$$E = \frac{HRR}{A} = \frac{HRR}{0.25\pi D^2 + \pi DH} \tag{3}$$

where HRR is the heat release rate (kW), A is the flame surface area (m^2), H is the flame height (m), and D is the flame diameter (m).

The geometric view factor (F) between the flame centre and the target is given below:

$$F = \begin{cases} \dfrac{H(D/2)^2}{2(L^2+H^2)^{3/2}} & L \le D/2 \\ \dfrac{L(D/2)^2}{(L^2+H^2)^{3/2}} & L > D/2 \end{cases} \tag{4}$$

where L is the horizontal distance from the flame surface to the exposed target (m).

The atmospheric transmissivity τ subject to the distance *s* can be defined as Equation (5) [59].

$$\tau = 1.389 - 0.135 * \log_{10}\left[p_w^{sat}(T_a)s\right] \tag{5}$$

where $p_w^{sat}(T_a)$ is the water vapor partial pressure under the environment temperature T_a (N/m^2), which can be calculated as $p_w^{sat}(T_a) = 101325 * (RH/100)\exp\left[14.4114 - \left(5328.1/T_a\right)\right]$, T_a is the environment temperature, which is often defined as 273~303 K; and RH denotes the relative humidity of the atmosphere (%), which is often defined as 40~70 %. In this study, the relative humidity of the atmosphere is defined as 70 %, $RH = 70$, and the environment temperature is defined as 300 ($T_a = 300k$) [55]. Therefore, the water vapor partial pressure is given by: $p_w^{sat}(T_a) = 101325 \times 0.7 \times \exp(14.4114 - 5328/300) = 2491.93$. Then, the atmospheric transmissivity can be represented by τ .

$$\tau = 1.389 - 0.135 * \log_{10}\left[p_w^{sat}(T_a)s\right] = 1.389 - 0.135 \times \log_{10}(2491.93 * s) \tag{6}$$

Equation (6) indicates that the atmospheric transmissivity τ decreases exponentially with distance *s*. The value of atmospheric transmissivity at different distances s can be calculated by Equation (6), as shown in Table 1.

Table 1 Atmospheric transmissivity

Distance (m)	τ	Distance (m)	τ	Distance (m)	τ
0.35	0.9930	0.85	0.9409	1.6	0.9039
0.4	0.9851	0.9	0.9376	1.7	0.9003
0.45	0.9782	0.95	0.9344	1.8	0.8970
0.5	0.9721	1	0.9314	1.9	0.8938

0.55	0.9665	1.05	0.9286	2	0.8908
0.6	0.9614	1.1	0.9258	2.5	0.8777
0.65	0.9567	1.2	0.9207	3	0.8670
0.7	0.9523	1.3	0.9160	4	0.8501
0.75	0.9483	1.4	0.9117	5	0.8371
0.8	0.9445	1.5	0.9076	10	0.7964

2.2.3 Spatial distribution of thermal radiation

This section defines the core parameters (flame height, diameter, and radiant power) that govern the fire models and subsequently apply the PSM and SFM to quantify the thermal radiation flux to the surroundings.

(1) Sample battery and data acquisition

Wang et al. [52] conducted a set of experiments to study the burning behaviour of LIBs, especially $LiFePO_4$. According to the literature [53], the nominal capacity of the LIBs used in the experiment is 50 Ah. Each battery comprises 5 small battery cells connected in series. The size of each battery is 0.353×0.1×0.028 m, with a weight of 1675 g.

Note that the SOC of an LIB is an essential factor for fire radiation. The HRR and toxic gases productions depend strongly upon the SOC level. The SOC of an LIB is a critical factor in chemical reactions, and maintaining an SOC below 50 % is essential for mitigating degradation and aging processes during transportation [60]. Traditionally, 100, 50 and 0 % SOC are chosen as the typical SOC values in studies.

According to [51], combustion behaviour can be categorized into three distinct stages: ignition, stable combustion, and termination. The flame size, HRR, and mass loss rate are time-varying. Burning experiments with 100 % SOC, 50 % SOC, and 0 % SOC LIBs were carried out.

Notably, the higher the SOC level is, the greater the HRR. This means that a fully charged LIB releases the highest radiative power with the largest flame size. The maximum flame size, HRR and maximum mass loss rate during the burning process are recorded in Table 2.

Table 2 Burning information of battery fire

SOC (%)	Flame Height (m)	Flame Diameter	HRR (kW)	Maximum mass loss rate (g/s)
100	0.257	0.304	64.32	8
50	0.254	0.275	55.93	3.983
0	0.309	0.109	20.65	3.583

In thermal radiation safety analysis, the worst-case scenario should be considered. For a given battery, the highest SOC should be chosen to calculate the safety distance. Table 1 shows that the flame height and diameter of the LIBs with 100 % SOC are 0.257 and 0.304 m, respectively; the radiative heat is 64.32 kW; and the maximum mass loss rate is 8 g/s.

(2) Application of the PSM and SFM

In this section, both the PSM and SFM are used to determine the thermal radiant distribution of the aforementioned sample battery. Supposing that a target is located at a distance s from the flame, the thermal radiation flux that the target suffers from the burning battery can be obtained.

According to the reported results of sample battery burning test, the values of parameters in the PSM and SFM can be identified. For the PSM, Q in Equation (1) is 64.32, 55.93, and 20.65 kW for batteries with 100 % SOC, 50 % SOC, and 0 % SOC, respectively. Thus, the thermal radiation flux that the target suffers from the burning battery can be obtained under different SOC levels by Equation (1). For the SFM, three key parameters in equation $q''(s) = E \cdot F(s)\tau(s)$ are determined, namely, the mean surface emissive power (E), atmospheric transmissivity (τ) and view factor (F).

The value of mean surface emissive power (E) can be calculated by using Equation (3). For a given point outside the battery, the size of the battery is 0.353×0.1×0.028 m. Supposing that the distance from the flame

centre to the exposed target s meets the following requirement: $s>0.353>D/2$, the view factor can be calculated as $F=s(D/2)^2/(s^2+H^2)^{3/2}$. The mean surface emissive power (E) of the fire at 100 % SOC, 50 % SOC and 0 % SOC can be calculated as 120.2, 121.01, and 49.26 kW/m^2, respectively. For a given point, the flame size value is assigned to the parameter in the equation for F ,and the view factor can also be obtained for 100 % SOC, 50 % SOC, and 0 % SOC.

Based on the atmospheric transmissivity shown in Table 1, the thermal radiation flux that the target suffers from the burning battery can be obtained under different SOC levels by Equation (2). Therefore, the thermal radiation flux can be calculated via the PSM and SFM at different distances for different SOC levels. Figure 3 shows the thermal radiation flux distribution of different distances for 100 % SOC, 50 % SOC, and 0 % SOC according to the PSM and SFM models.

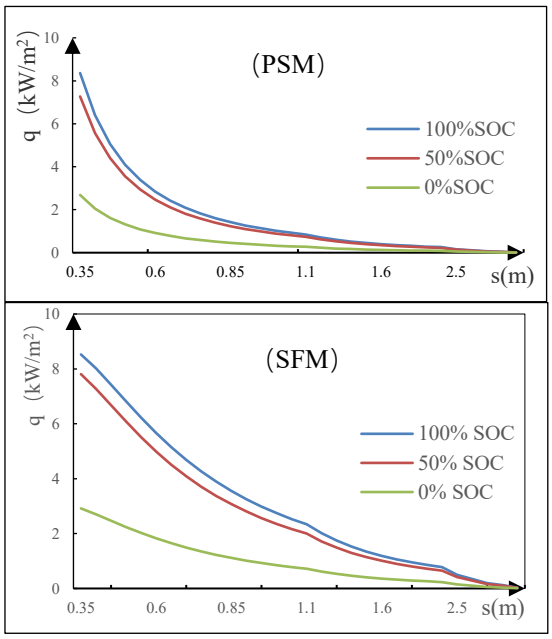

Fig. 3. Thermal radiation fluxes at different distances

As shown in Figure 3, the thermal radiation flux increases as the SOC level increases at a given point outside the flame. For a given SOC level, the farther away from the target, the smaller thermal radiation flux is. The radiant heat flux decreases dramatically as the distance increases in the range of 0.35 to 0.85 m, as calculated using the PSM.

A comparison of the results of the two models reveals that the thermal radiation flux distribution is generally consistent, with little difference in the extent of variation. The thermal radiation flux varies from more than 8 to 0 W/m^2 as the distance increases from 0.35 to 10 m. For a given point outside the flame, the higher the SOC level is, the greater thermal radiation flux. However, the thermal radiation flux of the SFM is slightly greater than that of the point source model.

(3) Distance for preventing radiation

The key safety concern on battery fire is the thermal radiation to surroundings. This section investigates the spatial distribution of the thermal radiation generated during a battery fire to determine the minimum safety distance for preventing radiation damage to personnel and surrounding equipment. The experimental results from Sandia National Laboratories show that the acceptable thermal radiation flux for people is 5 kW/m^2 [58]. For a ship steel structure building, the acceptable thermal radiation flux is 15 kW/m^2. By defining the acceptable thermal radiation flux as the threshold level, the safety distance required to prevent radiation damage can be determined. Taking the personnel safety distance as an example, when the acceptable thermal radiation threshold for humans is set to 5 kW/m^2, the corresponding safety distance calculated by the PSM at 100 % SOC (Table 2) is 0.45 m. This indicates that exposure to radiant heat that exceeds safe limits would occur if a person were within 0.45 m of the burning battery.

2.3 Battery-powered ship safety distance

2.3.1 Longitudinal safety distance based on following theory

Ship following theory was introduced for ship longitudinal safety distance analysis [58]. To avoid collisions between battery-powered ships and other ships, this study applies following theory to calculate the longitudinal safety distances of battery-powered ships. As the longitudinal safety distance of a ship is influenced by the following ship, the battery-powered ship is defined as the following ship in this study.

Suppose that the battery-powered ship is the following ship. The scenario is presented in Figure 4. In this situation, the following ship (ship A) begins to brake and decelerate at a certain moment, and the battery-powered ship (ship B) also starts to brake after a reaction period. During the reaction period, the battery-powered ship maintains its normal speed. Afterward, the following ship completed braking, and the battery-powered ship finished braking after a few minutes. Finally, the two ships navigate at the same ship speed.

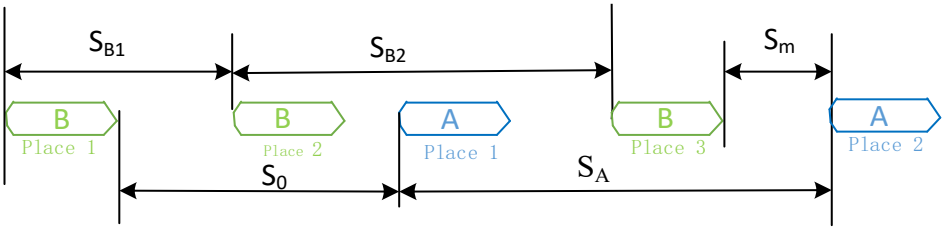

Fig. 4. Schematic diagram of the battery-powered ship according to following theory

Ship B is the battery-powered ship, and ship A is the following ship

S_0 : The initial distance between ship B and ship A.

S_{B1} : The sailing distance of ship B during the reaction period.

S_{B2} : The sailing distance of ship B for braking.

S_A : The sailing distance of ship A for braking.

S_m : The final distance between ship B and ship A when they stop.

From Figure 4, the safety distance can be calculated by Equation (7).

$$S_0 = S_{B1} + S_{B2} + S_m - S_A \tag{7}$$

The safety distance is the minimum initial distance for avoiding a collision. For the conventional ship, when $S_m = 0$, S_0 denotes the safety distance. For the battery-powered ship, S_m indicates the minimal distance for avoiding radiation. The greater the safety distance is, the safer the ship is. In practice, the crews always prefer large spaces, if possible. Therefore, it is meaningful to discover the maximum S_0 . $S_A \approx 0$ from a previous study [61]. Therefore, the safety distance can be calculated by the formula $S_0^* = S_{B1} + S_{B2} + S_m$, where $S_{B1} = Vt$, V is the initial speed of ship B, and t is the reaction time, which is usually defined as 10~20 s.

Ship braking can be divided into parking braking and back braking. The back braking distance is significantly less than the parking braking distance, and the braking distance of a ship is applied for safety zone calculation in this study to derive a large space.

The parking brake stroke S_{B2} can be estimated by the empirical formula proposed by Captain Topley.

$$S_{B2} = 0.024C \times V \times 1852 \tag{8}$$

where, S_{B2} represents the ship parking stroke (m), C denotes the time constant of ship speed halving (min), which varies with the displacement of the ship, as illustrated in Table 3, and V is the initial speed when the ship is parking (kn).

Table 3 Time constant of ship speed halving (C) [58]

Displacement (t)	C (min)	Displacement (t)	C (min)
1000	1	~45000	9
~3000	3	~55000	10
~6000	3	~66000	11
~10000	4	~78000	12
~15000	5	~91000	13
~21000	6	~105000	14
~28000	7	~120000	15
~35000	8		

Therefore, the longitudinal safety distance for a battery-powered ship is expressed as follows:

$$S_0 = Vt + 0.024C \times V \times 1852 + S_m \tag{9}$$

where S_m indicates the minimal distance for avoiding radiation r^*. In summary, for a battery-powered ship, as depicted in Figure 3, the longitudinal safety distance can be obtained by the following formula:

$$a = Vt + 0.024C \times V \times 1852 + r^* \tag{10}$$

The formula indicates that the longitudinal safety distance is related to ship speed, displacement and reaction time.

2.3.2 Lateral safety distance based on the classic ship domain model

The width of the ship domain should effectively avoid side collisions and deviations. Ship and shore suction are two important factors used to define the lateral safety distance for ship navigation.

For two ships sailing in parallel, if the lateral distance is too close, one will be attracted or repelled by the other due to hydrodynamic action. In this way, the affected ship may deviate from the normal route. Therefore, the lateral distance should be not less than the sum of the two ships' widths. When a ship is sailing near the shore, the fluid flow on the left and right sides is asymmetrical. The hull is subjected to a lateral force directed to the quay wall, and the ship bow deflects from the quay wall, which results in shore suction. The appropriate range of horizontal distance is 1.5~2L (the ship length is given as L) to avoid shore suction [62].

Owing to the limitations of endurance and electric power technology, battery-powered ships are currently used mainly in inland waterways. For conventional ships, several classical ship domain models [54] empirical methods have been proposed. The ship domain's width is 1.75L for the left sector, and 1.75L for the right sector [18]. In this study, 3.2L is defined as the safety distance to avoid side collisions and deviations. Therefore, a battery-powered ship, as depicted in Figure 3, the width of the ship safety exclusion zone can be defined as $2b$=2(1.6L+r^*).

3. Case study and result analysis

3.1 Data description

In this section, a case study is conducted to demonstrate the proposed method by using the battery-powered ship "Yangtze River Channel battery 001" as an example. "Yangtze River Channel battery 001" is the first 18 m pure battery-powered ship certified by the China Classification Society for the Yangtze River. The ship is used for channel maintenance, and the details of the ship are shown in Table 4.

Table 4 Details of the battery-powered ship "Yangtze River Channel battery 001"

Category	Value
Length, L	18.9 m
Breadth, B	4.2 m
Depth	1.7 m
Draft	0.9 m
Capacity of battery	1290 kWh
Endurance	6 h
Design speed	21.5 km/h

The battery cell described in Section 3.2.3 is 50 Ah, the nominal voltage is 3.2 V, and the ship battery consists of 8062 battery cells. Variations in combustion dynamics alter the spatiotemporal distributions of temperature and thermal radiation intensity, thereby affecting the determination of safety exclusion distances. Thus, a systematic investigation of battery combustion under various scenarios is imperative for establishing safety exclusion zones for battery-powered ships. Typically, when the SOC level of the battery is lower than 20 %, the ship is required to dock at the charging station for battery replenishment. Therefore, the scenario in which 0 % SOC level of the battery (which is less than 20 %) is not considered. As the radiative power of the ship battery is the sum of the radiative power of the battery cells, the radiative power of the ship battery can be calculated as 518547.8 and 450907.7 kW for batteries with 100 % SOC and 50 % SOC, respectively.

3.2 Thermal radiation of ship battery fires

In this section, the PSM and SFM are used to calculate the radiant heat flux to the surroundings in the event of a fire accident. The safety distance for avoiding thermal radiation can be determined according to the spatial distribution of thermal radiation with acceptable thermal radiation flux.

3.2.1 Spatial distribution of thermal radiation obtained via the PSM and SFM

Similar to the analysis of spatial distribution of thermal radiation for the sample battery cell in Section 2.2.3, the values of the parameters in the PSM and SFM can be identified.

For the PSM, Q in Equation (1) is 518547.8 and 450907.7 kW for the batteries with 100 % SOC and 50 % SOC, respectively. Thus, the thermal radiation flux varies from 12 to 44 m. The results are shown in Table 4.

According to the details described in Section 3, the atmospheric transmissivity (τ) is given, and the radiation power is known. For the SFM, to derive the values of the mean surface emissive power (E), and the view factor (F), the size of the flame should be determined. As there is no combustion test for containerized batteries, the size of the flame should be deduced by logical and theoretical reasoning. Traditionally, the flame diameter is related to the size of the fire source. To simplify the study, the ship battery can be considered as an equivalent sphere of the same size. The diameter of the sphere is 4.13 m according to the SFM model, which is also considered to be the diameter of the flame for the battery burning under 100 % SOC. According to the change law of the diameter with the SOC level, the flame diameter is predicted to be 3.70, 3.92 and 4.13 m.

Many authors have studied the relationship between flame height (H) and diameter (D) through experimental and theoretical approaches [63, 64], but the length and width correlations are still uncertain owing to the different fuels and fire scales. However, for large scale flames,most H/D ratios fall within the range of 0.71~7.

In several large ship fire experiments, several values for the flame height-to-diameter ratio (H/D) have been obtained: 0.71, 0.822, 1.28, and 1.35 [59, 65]. Empirical analysis of vertically oriented propane jet flames demonstrated turbulent flame stabilization in cylindrical geometry with an aspect ratio H/D of 7 [66]. For flame diameters less than 12 m, the average length-diameter ratios are calculated as nearly 4 by three different flame shape models. As the fuel of a LIB is an ionic liquid, the burning behaviour could seem to be a fire that is somewhere between a pool fire and a jet fire. Thus, for the flame of the battery container considered in this study, the height-diameter ratio (H/D) is defined as the average value of the results listed above, namely, 2.52.

Therefore, the flame lengths are 9.32, 9.88, and 10.41 m for diameters of 3.70, 3.92, and 4.13 m, respectively. The parameters in the SFM can be calculated based on the flame size. The radiant heat flux is obtained as the distance varies from 12 to 44 m. The radiant heat flux distributions are shown in Table 5.

Table 5 Radiation heat flux (kW/m^2)

	PSM		SFM			PSM		SFM	
Distance (m)	100 %	50 %	100 %	50 %	Distance (m)	100 %	50 %	100 %	50 %
12	48.066	41.797	33.098	30.574	29	8.230	7.157	9.427	8.321
13	40.956	35.614	30.613	28.111	30	7.691	6.687	8.869	7.822
14	35.314	30.708	28.257	25.812	31	7.202	6.263	8.357	7.364
15	30.763	26.750	26.059	23.695	32	6.759	5.878	7.885	6.943
16	27.037	23.511	24.030	21.762	33	6.356	5.527	7.450	6.555
17	23.950	20.826	22.170	20.006	34	5.988	5.206	7.048	6.198
18	21.363	18.576	20.473	18.416	35	5.650	4.913	6.676	5.867
19	19.173	16.672	18.929	16.979	36	5.341	4.644	6.332	5.562
20	17.304	15.047	17.525	15.681	37	5.056	4.396	6.012	5.278
21	15.695	13.648	16.251	14.509	38	4.793	4.168	5.715	5.015
22	14.301	12.435	15.094	13.449	39	4.551	3.957	5.439	4.770
23	13.084	11.378	14.043	12.490	40	4.326	3.762	5.181	4.542
24	12.017	10.449	13.087	11.621	41	4.118	3.580	4.940	4.330
25	11.075	9.630	12.216	10.832	42	3.924	3.412	4.715	4.131
26	10.239	8.903	11.422	10.115	43	3.743	3.255	4.505	3.946
27	9.495	8.256	10.697	9.462	44	3.575	3.109	4.308	3.772
28	8.829	7.677	10.034	8.866					

Figure 5 shows the radiant heat flux distributions associated with the distance for 100 % SOC and 50 % SOC according to the two thermal radiation models. According to Table 5, the radiant heat flux decreases from 192.27 to 3.58 kW/m^2 as the distance increases from 12 to 44 m for 100 % SOC.

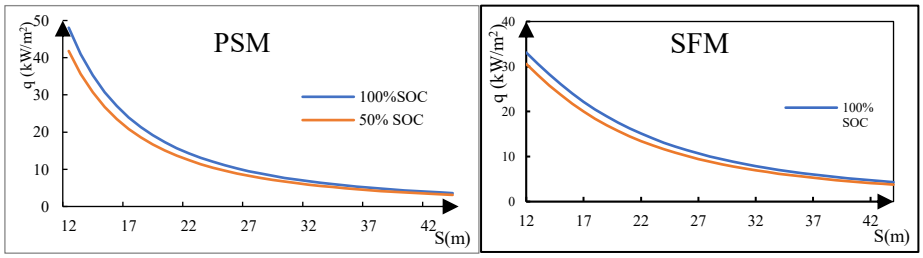

Fig. 5. Radiant power at different distances

Figure 5 shows that the radiant heat flux increases as the SOC level increases at a given point outside the flame. For the same SOC, as the distance from the fire center increases, the radiation power decreases. The thermal radiation spreads in all directions, and the radiation intensity that reaches a given target decreases as the distance from the flame surface increases at the same SOC level. As the level of the battery SOC increases, the radiation power for a certain distance becomes stronger. The radiation power clearly decreases significantly as the distance from the flame increases within the range of 8~20 m. The distance that is based on the acceptable thermal radiation flux is the safety distance for avoiding radiation. For 100 % SOC, the radiation power is more than 15 kW/m^2 when the distance is less than 21.72 m, and the radiation power ranges between 5 and 15 kW/m^2 when the distance is between 40.89 and 21.72 m. The radiation power is less than 5 kW/m^2 when the distance is far from 40.89 m.

3.2.2 Determination of the safety distance for avoiding thermal radiation

The acceptable thermal radiation flux for people is 5 kW/m^2, and the acceptable thermal radiation flux for ship steel structure building is 15 kW/m^2. By setting the acceptable thermal radiation flux as the threshold level, the safety distance for avoiding radiation damage can be determined. Table 6 shows the safety distances when the radiant heat flux is 5 and 15kW/m^2 according to the PSM and SFM models.

Table 6 The safety distance for people and ship by PSM and SFM (m)

	PSM		SFM	
radiation heat flux (kW/m^2)	100 % SOC	50 % SOC	100 % SOC	50 % SOC
5	36.97	35.12	40.89	38.98
15	20.53	19.86	21.72	21.38

Table 6 shows that the safety distance increases as the SOC level increases. As the safe thermal radiation flux for people should be less than 5 kW/m^2, the safety distance should be more than 36.97 and 35.12 m for 100 % SOC and 50 % SOC, respectively, according to PSM. The safety distance should be more than 40.89 and 38.98 m for 100 % SOC and 50 % SOC, respectively, according to the SFM. As the safe thermal radiation flux for ship steel structure buildings should be less than 15 kW/m^2, the safety distance should be more than 20.53 and 19.86 m for 100 % SOC and 50 % SOC, respectively, according to the PSM. The safety distance should be more than 21.72 and 21.38 m for 100 % SOC and 50 % SOC, respectively, according to the SFM.

Therefore, the safety distance estimated by the SFM is slightly greater than that estimated by the PSM. According to the research by B. J. Lowesmith et al. [67], when the distance is greater than twice the flame length, the flame shape is not critical. In this study, the safety distances calculated by the two models are more than twice the flame length and five times the flame diameter. Therefore, the two models are applicable. Additionally, the difference in the safety distances calculated by the two models is less than 19 %. Therefore, it is considered that the results of the two models are consistent. The method of taking the average value can integrate the results of both, effectively reducing the errors caused by a single model and improving reliability. To analyse the results of the two models, comprehensively, the average value is also calculated to obtain an appropriate safety distance, which is shown in Table 7.

Table 7 The average safety distance for people and ship (m)

radiation heat flux （kW/m^2）	100 % SOC	50 % SOC
5	38.93	37.05
15	21.12	20.62

3.3 Simulation analysis

3.3.1 Arrangement of monitoring points

To clarify the distributions of heat and temperature, FDS 6.7 software is used for simulation. Sixteen temperature and radiation sensors are positioned around the vessel perimeter, as indicated by the yellow markers in Figure 6. There are eight horizontal detection points: +X1, +X2, +X3, +X4, -X1, -X2, -X3, and -X4. There are eight vertical detection points: +Y1, +Y2, +Y3, +Y4, -Y1, -Y2, -Y3, and-Y4. The distance between each detection point is set to be 2.5 m. The rationale behind this arrangement rests on two principal considerations. Firstly, the 2.5 m spacing is optimized to resolve the differential thermal-radiation flux between adjacent sensors with high fidelity. Smaller pitches produce negligible flux changes, increasing costs without benefit, while larger pitches lose critical gradients and prevent accurate thermal-field reconstruction. Secondly, the configuration guarantees complete coverage of a 10 m band along each side of the vessel—the core zone defined by safety-distance criteria. Within 10 m, thermal-radiation flux varies significantly, enabling precise thermal-field mapping through detectable and quantifiable gradients.

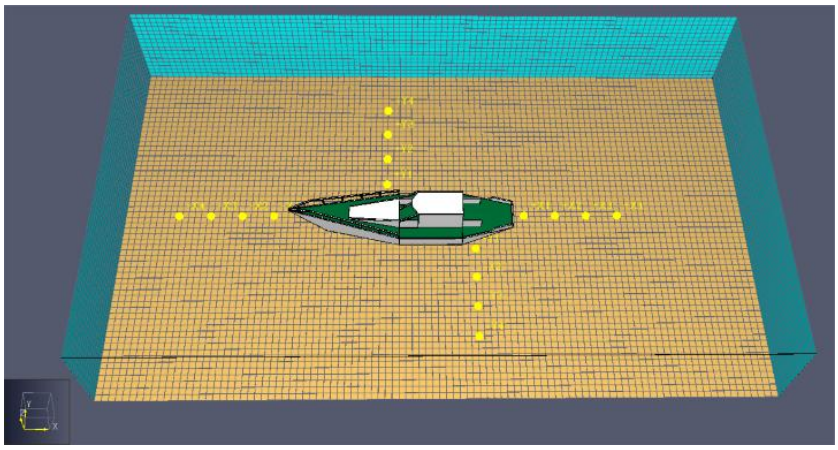

Fig. 6. Arrangement of monitoring points around the sample ship "Yangtze River Channel battery 001"

3.3.2 Heat release rate

This software is used to simulate the battery combustion process, and the heat release rate during the burning time is shown in Figure 7. The heat release rate peaks at approximately 205 s.

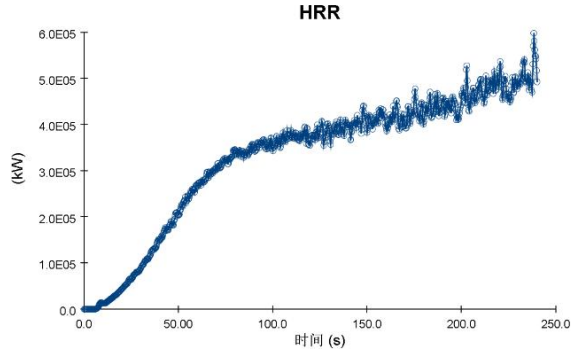

Fig. 7. Heat release rate curve

The time variation curves of the thermal radiation flux at the X-direction and Y-direction detection points are shown in Figures 8 and 9, respectively.

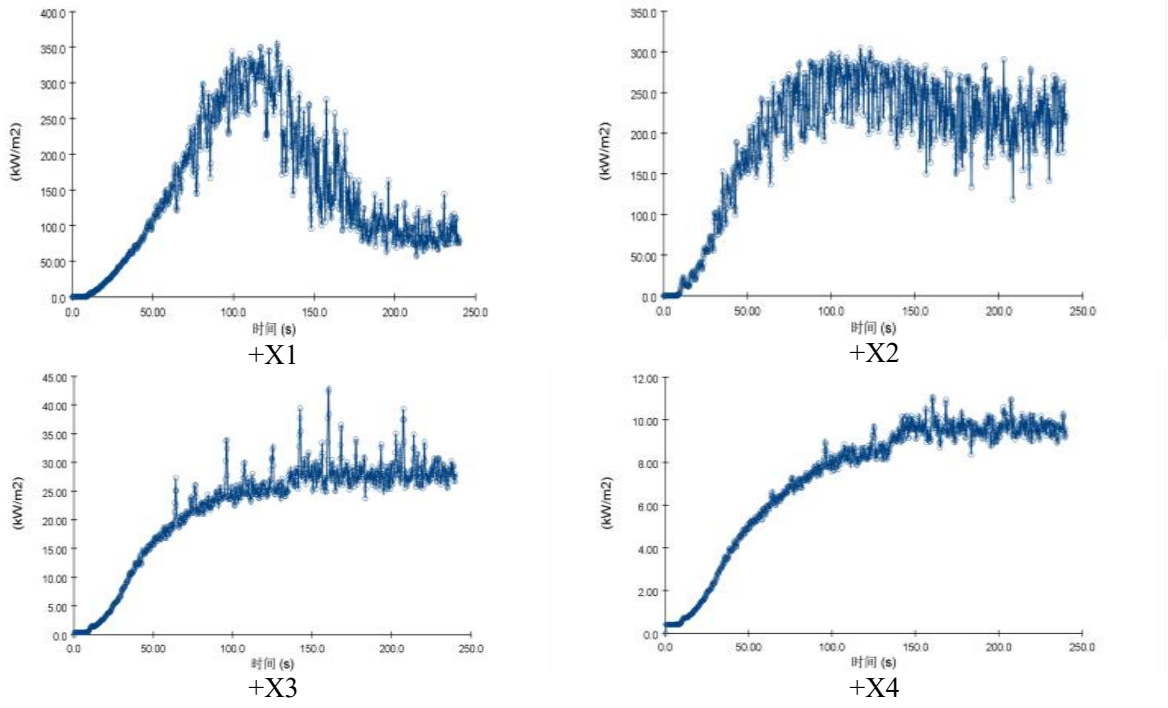

Fig. 8. Simulation model of "Yangtze River Channel battery 001"

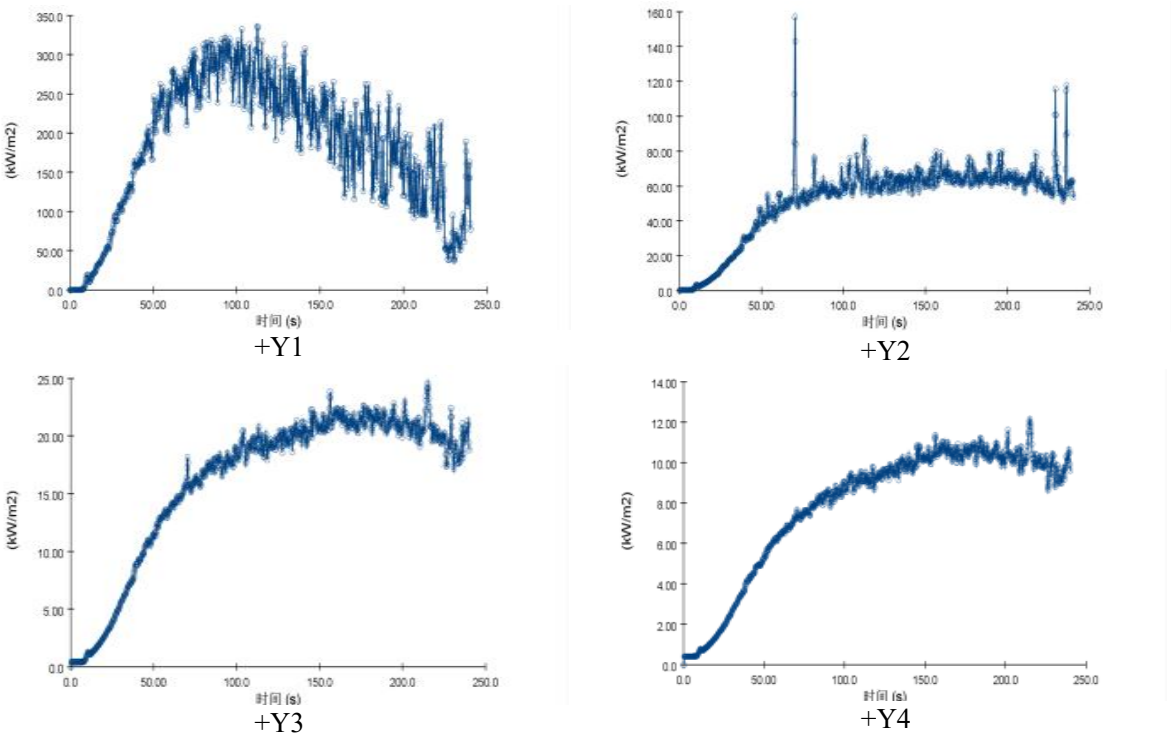

Fig. 9. Time variation curves of the thermal radiation flux in +Y direction

3.3.3 Temporal and spatial distributions

The temporal and spatial distributions of the battery ship fire temperature are shown in Figure 10.

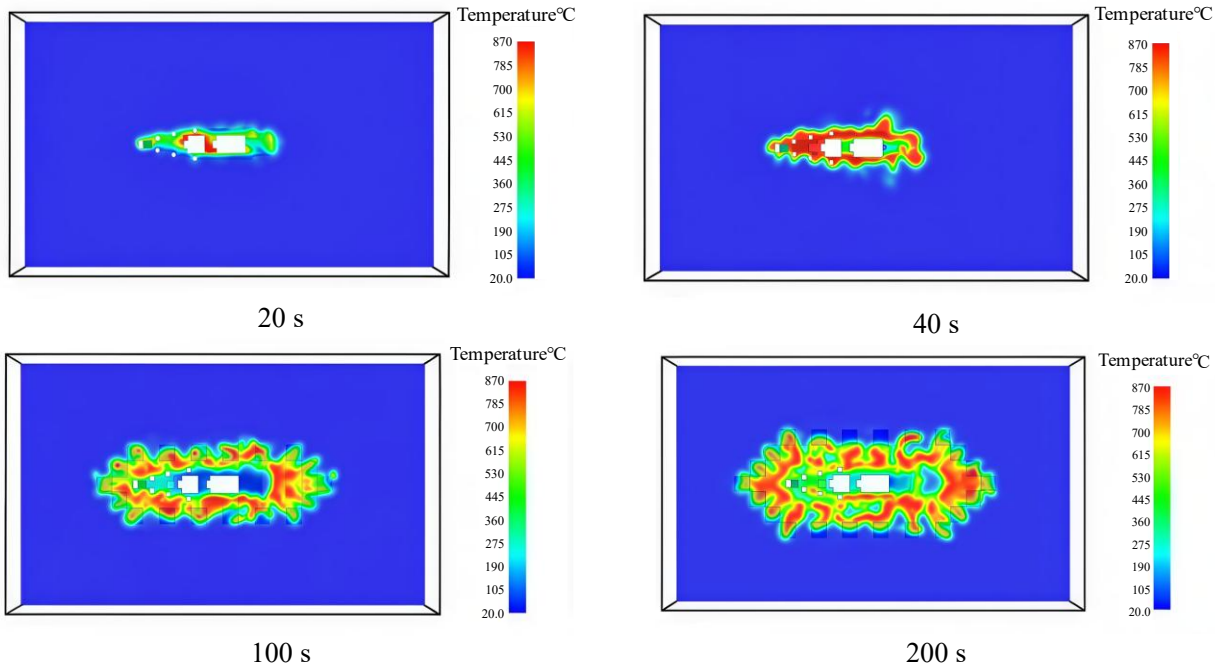

Fig. 10. Temporal and spatial distributions of the battery ship fire temperature

At approximately 200 s, the ship fire temperature peaks, and the temperature rises from 20 °C to 785 °C.

3.3.4 Temperature and heat flux distributions under different SOCs

Figures 11 and 12 show the temperature and radiation heat flux distributions under different SOCs.

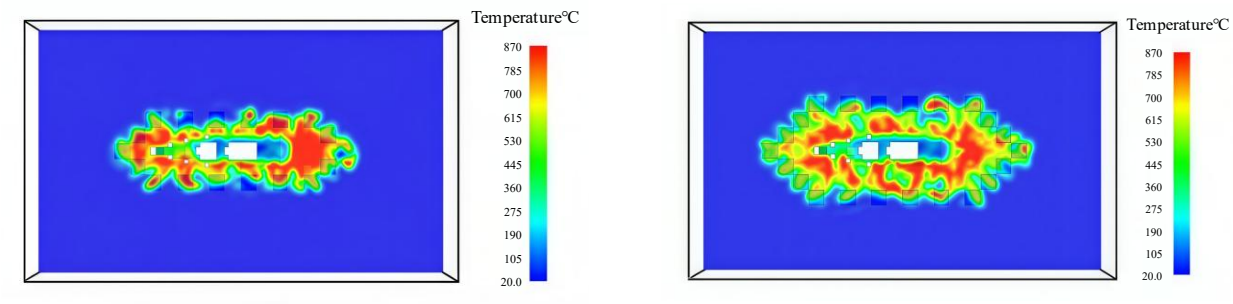

50 % SOC **100 % SOC**

Fig. 11. Temperature distributions under 50 % and 100 % SOC

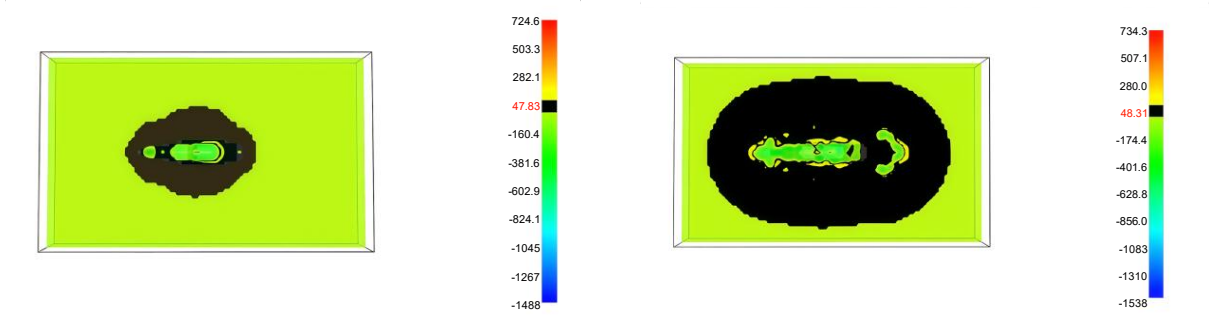

50 % SOC **100 % SOC**

Fig. 12. Radiant heat flux distributions under 50 % and 100 % SOC

(1) To guarantee the safety of nearby people, the thermal radiation flux of the people suffering should be less than 5 kW/m^2. Taking the SOC 100 % as an example, the thermal radiation flux at 38.93 m from the centre is 5 kW/m^2. This means that nearby people should maintain a distance of more than 38.93 m to avoid thermal radiation from the battery-powered ship.

(2) To guarantee the safety of nearby ships, the thermal radiation fluxes the ship suffering should be less than 15 kW/m^2. Taking the SOC 100 % for example, the thermal radiation flux at 21.12 m from the centre is 15 kW/m^2. This means the nearby ships should maintain a distance of at least 21.12 m to avoid thermal radiation from the battery-powered ship.

(3) For the safety of people, the maximum safety distance is 38.93 m. For ship safety, the maximum safety distance is 21.12 m. As the SOC level decreases, the safety distance of the ship decreases.

3.4 Determination of the battery-powered ship exclusion zone

According to the formula proposed in Section 3, the longitudinal safety distance of the ship can be calculated as $a = Vt + 0.024C \times V \times 1852 + r^*$,where C denotes the time constant for ship speed halving in Table 1. Since the displacement of the target ship is less than 1000 t, $C = 1$. t is the reaction time, and t is set 10s in this study. The parameter V describes the speed of the target ship. The formula indicates that the longitudinal safety distance is related to the ship speed. The maximum speed of the battery-powered ship is 21.5 km/h. The actual speed ranges from 5 to 15 km/h.

The parameter r^* is the safety distance for avoiding thermal radiation for the ship, as shown in Table 7. By setting the acceptable thermal radiation flux as the threshold level, the safety distance for avoiding radiation damage can be derived. In the worst-case scenario, namely, when the SOC of the battery is 100 %, r^* should be 38.93 and 21.12 m for safety for people and other ships, respectively. As stated in the previous section, the lateral safety distance of the battery-powered ship can be derived as $1.6L + r^*$, where L =18.9 m. Finally, the ship safety exclusion zones of the "Yangtze River Channel battery 001" that correspond to various speeds are shown in Table 8.

Table 8 Ship safety exclusion zones for "Yangtze River Channel battery 001"

Acceptable thermal radiation (kW/m^2)	Radiation safety distance r^* (m)	Speed v (km/h)	Longitudinal safety distance a^* (m)	Lateral safety distance b^* (m)
5	38.93	5	172.82	45.65
		6	199.6	45.65
		7	226.37	45.65
		8	253.15	45.65
		9	279.93	45.65
		10	306.71	45.65
15	21.12	5	155.01	27.84
		6	181.79	27.84
		7	208.56	27.84
		8	235.34	27.84
		9	262.12	27.84
		10	288.90	27.84

From Table 8, compared with a traditional ship, the safety distance should be extended by 21.12 m (38.93 m) for battery-powered ship for radiation avoidance. The longitudinal safety distance increases from 172.82 and 306.71 m as the speed increases from 5 to 10 km/h to guarantee the safety of ships nearby. The longitudinal safety distance increases from 155.01 and 288.90 m as the speed increases from 5 to 10 km/h to guarantee the safety of people. For example, when the ship speed is 8 km/h, people should maintain a longitudinal distance of 253.15 m. The ship lateral safety distance is subject to the radiation safety distance, which is unrelated to the ship speed. The safe lateral safety distances are 45.65 and 27.84 m for the safety of people and ships nearby, respectively.

As shown in Figure 13, when the ship speed is 8 km/h, the ship safety exclusion zones for people and other ships can be defined. Two blue ellipses describe the battery domain. The small deep blue ellipse zone represents the ship safety exclusion zone for ensuring people's safety, and the red circle inside represents the danger zone caused by thermal radiation. The outer larger light blue ellipse represents the ship safety exclusion zone for ensuring the safety of other ships, and the inner orange circular region represents the dangerous area caused by thermal radiation.

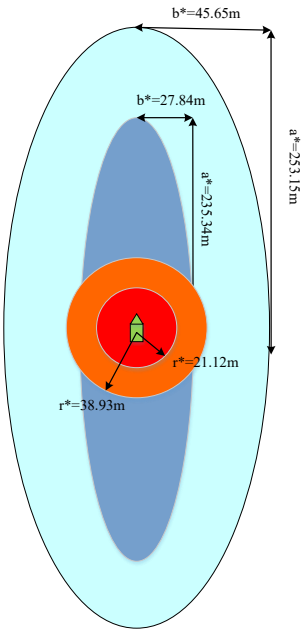

Fig. 13. Ship exclusion zone for "Yangtze River Channel battery 001"

3.5 Comparison and analysis of the results

This section conducts a comparative analysis based on existing regulations and literature to validate the proposed framework. Battery-powered ships, which have only entered operational service in recent years, lack sufficient historical fire incident data. As a result, traditional methods that rely on historical datasets or empirical accident cases are inadequate for verifying the effectiveness of this model. Nevertheless, LNG/ammonia-fuelled vessels, which are similarly classified as novel energy-powered maritime systems, have generated safety exclusion zone research that offers applicable references for battery-powered ships.

By conducting comparative analysis based on existing policies, this study demonstrates that its research conclusions align closely with current regulations on safety distances for new energy vessels. The conclusions of the case study are consistent with the real-world situation for new energy ships. For the safety of new energy ships, various regulations and provisions about safety exclusion zones have been issued. In Norway, maritime administration authorities have set up a 300 m safety zone around the battery-powered ship "MS Brim" to prohibit anyone from approaching in a fire accident. The Sandia National Laboratory in the United States proposed the concept of an LNG ship danger zone, which can be divided into several different levels. Among them, the most dangerous area is Zone I (Zone 1), which is 0~250 m around an LNG ship, followed by Zone II (Zone 2), which is 250~750 m around the LNG ship. The existing regulations concerning ship safety exclusion zones in some ports and countries are summarized in Table 9. Take a ship whose length is 24 m as an example. Figure 14 establishes the ship's centre as the coordinate origin, with the positive y-axis, negative y-axis, negative x-axis, and positive x-axis corresponding to the vessel's bow, stern, port, and starboard directions, respectively. Meanwhile, the regulations of new energy vessel safety exclusion zones in some nations are visualized through color-coded boundaries, reflecting variations in exclusion criteria.

Table 9 Summary of existing regulations about ship safety exclusion zone

Nation	Ship dangerous zone	Ship type	Source
Norway	300 m around the ship	Battery-powered ship (L=24 m, B=11 m)	Proposed by Norwegian Maritime Administration "MS Brim" Rescue practice and experience
France	Fore sector 2 nm, aft sector 2 nm	LNG ship	Rules conducted in Montoir de Bretragne Port
Canada	Fore sector 1 nm, aft sector 1 nm, left sector 250m, right sector 250 m	LNG ship	Proposed by Transport Canada's Atlantic Regional Marine Safety Committee
USA	250~750 m around the ship	LNG ship	Proposed by Sandia National Laboratory
USA	463 m around the ship	Non-specified Ship	Rules conducted in Chesapeake Bay (USA)
China	Fore sector 6L, aft sector 6L, left sector 4L, right sector 4L	LNG ship	International Ship and Port Facility Security Cod, conducted in Yangshan Port

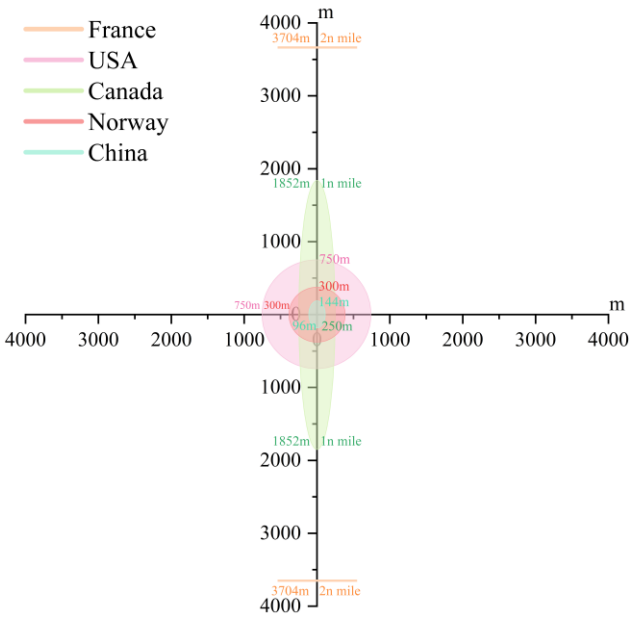

Fig. 14. Safety exclusion zone for new energy vessels in different countries

As shown in Table 9, the exclusion zone derived by this study is generally in line with the existing rules. Some ship safety zones shown in Table 9 are generally applicable, which could be tolerable for the ship considered in the case study. However, some distances are overly conservative and excessively vague for the case study ship, such as the critical distance of 250~750 m. Considering the ship type and the navigational waters, the first and last rules are more applicable for the case study ship. The longitudinal safety distance of the exclusion zone derived in this study is 9*L* (*L*/*B*=172.82 m / 18.9 m=9), which meets the requirements specified by the relevant rules, ranging from 6*L* to 12.5*L* (*L*/*B*=300 m / 24 m=1.25).

Table 10 Estimation of safety exclusion zone under various scenarios

Nation	Critical distances	Scenario description	Method and Reference
China	Farther than 60 m from the explosion site (Acceptable risk level)	Methanol fire and explosion Leakage rate is 0.0035 kg/s	HYSYS simulation [45]
China	Fore sector 24.8 m, aft sector 24.8 m, left sector 16.2 m, right sector 16.2 m	Hydrogen leakage and explosion accidents, Maximum explosion overpressure 50 kPa	FLACS-CFD simulation [42]
China	926 m around the ship	Declarative ship arenes for safe passing, ship size *L*=221.5 m, *B*=32 m	DCPA TCPA [36]
Korea	Fore sector 34.5 m, aft sector 34.5 m, left sector 5.6 m, right sector 5.6 m	LNG ship leakage Leak hole size 150 mm Ship size *L*=48.5 m, *B* =12.4 m	FLACS-CFD simulations [41]
Korea	Fore sector 73.5 m, aft sector 73.5 m, left sector 11.7 m, right sector 11.7 m	NH_3 ship leakage Leak hole size 150mm Ship size *L*=48.5 m, *B* =12.4 m	FLACS-CFD simulations [41]
China	Farther than 8.15 m from the fire (Acceptable risk Area)	Spill fire in sealed ship Ship size *L*=9 m, *B*=9 m Average HRR=30 J/s	Experimental [15]
UK	Farther than 541.8 m from the ship (10^6/year criterion)	LNG ship leakage Ship size *L*=190.6 m, *B*= 32.0 m leak hole diameter 150 mm	CFD simulation [39][40]

Further comparative analysis reveals findings that are in line with recent scholarship on new energy ship safety distances. Many researchers have carried out experiments and simulation studies to determine safety exclusion zones under various scenarios, such as open or restricted water, different wind speeds or directions, varying leakage rates or heat release rates, and different types of energy, e.g., hydrogen, NH3, LNG, and batteries. Concerning the individual risk of fatality, Jeong et al. [40] suggested that a suitable threshold for the safe zone is 541.8 m under the 106/year criterion for LNG bankers. Table 10 presents the research results compiled from the relevant technical literature.

The radiation distance derived by this study is in line with the relevant technical literature. Table 10 presents the threshold safety distance for avoiding the hazards posed to equipment by energy fires or leakages. Since the critical distances are calculated based on energy characteristics and diversity scenarios, the acceptable-safety zones are not uniform. However, the radiation distance generally varies within the range of 1*L* (*L*/*B*=8.15 m / 9 m=0.91) ~ 2.84*L* (*L*/*B*=541.8 m / 90.6 m=2.84), with values of 8.15~541.8m. The radiation distance derived in this study is 38.93 m, 2.06*L* (*L*/*B*=38.93 m / 18.9 m=2.06) is almost the average value for the different types of energy and scenarios mentioned above.

In summing, the results derived from the case study are consistent with current studies and regulations concerning new energy ships in some countries and ports, as discussed in the aforementioned analyses. Therefore, the proposed method for analysing the battery-powered ship exclusion zone is shown to be rational and effective.

4. Conclusions

The kernel of this paper is to propose a simple but innovative approach for determining the safety exclusion zones of battery-powered ships. Since the concept and design methodologies for safety exclusion zones for battery-powered ships have not yet been standardized or generalized, this study provides critical insights for policymakers and researchers in advancing maritime safety protocols.

Based on an analysis of the safety requirements for battery-powered ships in case of fire accidents, a safety exclusion zone was designed for avoiding both collisions and thermal radiation damage. Two classic thermal radiation models were employed to investigate the spatiotemporal distribution of thermal radiation. By setting the acceptable thermal radiation flux (e.g., 5, 15 kW/m^2) as the threshold level, the safety distances under different State of Charge (SOC) levels for avoiding radiation damage were determined. Following theory and a classic ship domain model were applied to calculate the safety distance avoiding collision damage. In this sense, the size of the safety exclusion zone of a battery-powered ship is the safety distance for avoiding collisions plus the safety distance for avoiding radiation. The battery capacity, SOC level, and ship speed critically influence the safety exclusion zones. As personnel safety demands stricter requirements, the exclusion zone for vessel operations is smaller than that for human safety. Using CFD and FDS 6.7 fire simulation software, a case study of a battery-powered ship operating in the Yangtze River was conducted to validate the proposed methodology. Under a speed of 8 km/h speed and 100 % SOC, safety exclusion zones were established at (45.65, and 253.15 m) for personnel and (27.84 and 235.34 m) for ships nearby. According to a comparative analysis, the results derived from the case study are consistent with those of current studies and regulations on new energy ships.

Although this study has demonstrated the application of the proposed method, the accuracy of the safety exclusion zone model could be affected by the battery type, ship type, and ship operating conditions. In addition, the safety exclusion zone may also be related to several environmental factors, such as wind speed, flow velocity, and ambient temperature, which are not considered in this work because of the previous studies and incomplete data. Water body characteristics significantly influence safety requirements for battery-powered vessels, with distinct exclusion zones mandated across lakes, inland waterways, and open seas. The method for determining the safety exclusion zone proposed in this study has not yet been verified for its general applicability. Therefore, it will be meaningful to further develop the model and adjust to improve the model validation and the accuracy of the results based on more comprehensive consideration.

ACKNOWLEDGMENTS

This research is funded by the National Natural Science Foundation (No 52301422) and the Fund of State Key Laboratory of Maritime Technology and Safety (No 28-19-1), the Key Research Institute of Humanities and Social Sciences in Universities of Hubei Province (DSS20190104), Philosophy and Social Sciences Research Project of Hubei Provincial Department of Education (No 24Q096).

REFERENCES

[1] Pan, P., Sun, Y., Yuan, C., Yan, X., Tang, X., 2021. Research progress on ship power systems integrated with new energy sources: A review. *Renewable and Sustainable Energy Reviews*, 144, 111048. https://doi.org/10.1016/j.rser.2021.111048

[2] Wu, Y., Yang, B., Zhang, X., Ying, S., 2024. Research progress in battery thermal management system under vessel working conditions. *Journal of Energy Storage,* 96, 112761. https://doi.org/10.1016/j.est.2024.112761

[3] Yan, X., He, Y., Fan, A., 2023. Carbon footprint prediction considering the evolution of alternative fuels and cargo: A case study of Yangtze river ships. *Renewable and Sustainable Energy Reviews*, 173, 113068. https://doi.org/10.1016/j.rser.2022.113068

[4] Meng, L., Gan, H., Liu, H., Lu, D., 2025. Deep learning-based research on fault warning for marine dual fuel engines. *Brodogradnja*, 76(3), 76303. https://doi.org/10.21278/brod76303

[5] Meng, H., Hu, M., Kong, Z., Niu, Y., Liang, J., Nie, Z., et al., 2024. Risk analysis of lithium-ion battery accidents based on physics-informed data-driven Bayesian networks. *Reliability Engineering & System Safety*, 251, 110294. https://doi.org/10.1016/j.ress.2024.110294

[6] Guo, C., Utne, I. B., Zadeh, M., 2025. Real-time risk monitoring of autonomous all-electric ships' battery systems based on risk indicator data. *Journal of Marine Engineering & Technology*, 24(3), 228-240. https://doi.org/10.1080/20464177.2025.2487326

[7] Kong, L., Luo, Y., Fang, S., Niu, T., Chen, G., Yang, L., et al., 2025. State estimation of Lithium-ion battery for shipboard applications: Key challenges and future trends. *Green Energy and Intelligent Transportation*, 4(3), 100192. https://doi.org/10.1016/j.geits.2024.100192

[8] Wang, Y., Lu, X., Zhang, Y., Liu, L., 2024. Thermal runaway behaviour and heat generation optimization of the marine battery cabinet based on module thermal analysis. *Applied Thermal Engineering*, 240, 122188. https://doi.org/10.1016/j.applthermaleng.2023.122188

[9] Yan, Y., Wang, L., Wu, Z., Dong, J., Yuan, Z., Han, J., et al., 2024. Thermal runaway and combustion of lithium-ion batteries in engine room fires on oil/electric-powered ships. *Applied Thermal Engineering*, 254, 123838. https://doi.org/10.1016/j.applthermaleng.2024.123838

[10] Yin, R., Du, M., Shi, F., Cao, Z., Wu, W., Shi, H., et al., 2024. Risk analysis for marine transport and power applications of lithium ion batteries: A review. *Process Safety and Environmental Protection*, 181, 266-293. https://doi.org/10.1016/j.psep.2023.11.015

[11] Yang, L., Yang, J., Fan, A., Zhou, R., Wang, L., 2025. Fire risk assessment of electric ships on inland waterway based on GT-FFTA: A case study of China. *Ocean Engineering*, 332, 121329. https://doi.org/10.1016/j.oceaneng.2025.121329

[12] Gu, Y., Ni, H., Li, Y., 2024. Early-Stage ISC Fault Detection for Ship Lithium Batteries Based on Voltage Variance Analysis. *Machines*, 12(5), 303. https://doi.org/10.3390/machines12050303

[13] Liu, Y., Jin, H., Yang, X., Tang, T., Song, Q., Chen, Y., et al., 2024. Early Fault Diagnosis and Prediction of Marine Large-Capacity Batteries Based on Real Data. *Journal of Marine Science and Engineering*, 12(12), 2253. https://doi.org/10.3390/jmse12122253

[14] Wang, T., Li, Y., Zeng, Y., Zhang, G., Zhao, G., Li, X., et al., 2024. Investigation on the battery thermal management and thermal safety of battery-powered ship with flame-retardant composite phase change materials. *Journal of Energy Storage*, 81, 110228. https://doi.org/10.1016/j.est.2023.110228

[15] Wang, Z., Wang, Y., Shi, C., Liu, J., Wang, J., Li, J., et al., 2025. Combustion efficiency analysis and thermal radiation risk quantification for spill fire in sealed ship cabin. *International Journal of Thermal Sciences*, 208, 109449. https://doi.org/10.1016/j.ijthermalsci.2024.109449

[16] Zhou X., 2024. Spatial risk assessment of maritime transportation in offshore waters of China using machine learning and geospatial big data. *Ocean & Coastal Management*, 247, 106934. https://doi.org/10.1016/j.ocecoaman.2023.106934

[17] Szlapczynski, R., Szlapczynska, J., 2016. An analysis of domain-based ship collision risk parameters. *Ocean Engineering*, 126, 47-56. https://doi.org/10.1016/j.oceaneng.2016.08.030

[18] Szlapczynski, R., Szlapczynska, J., 2017. Review of ship safety domains: Models and applications. *Ocean Engineering*, 145, 277-289. https://doi.org/10.1016/j.oceaneng.2017.09.020

[19] Szlapczynski, R., Szlapczynska, J., 2021. A ship domain-based model of collision risk for near-miss detection and Collision Alert Systems. *Reliability Engineering & System Safety*, 214, 107766. https://doi.org/10.1016/j.ress.2021.107766

[20] Du, L., Banda, O. A. V., Huang, Y., Goerlandt, F., Kujala, P., Zhang, W., 2021. An empirical ship domain based on evasive maneuver and perceived collision risk. *Reliability Engineering & System Safety*, 213, 107752. https://doi.org/10.1016/j.ress.2021.107752

[21] Kundakci B., Nas S., Gucma L., 2023. Prediction of ship domain on coastal waters by using AIS data. *Ocean Engineering*, 273, 113921. https://doi.org/10.1016/j.oceaneng.2023.113921

[22] Pietrzykowski, Z., Wielgosz, M., 2021. Effective ship domain–Impact of ship size and speed. *Ocean Engineering*, 219, 108423. https://doi.org/10.1016/j.oceaneng.2020.108423

[23] Zhang, L., Gu, K., Ma, Z., Liu, J., Liu, S., Song, J., 2024. A spatiotemporal pattern analysis of cross encounter behaviour of ships based on Automatic Identification System data and a nearest point approach. *Ocean & Coastal Management*, 254, 107194. https://doi.org/10.1016/j.ocecoaman.2024.107194

[24] Silveira, P., Teixeira, A. P., Soares, C. G., 2022. A method to extract the Quaternion Ship Domain parameters from AIS data. *Ocean Engineering*, 257, 111568. https://doi.org/10.1016/j.oceaneng.2022.111568

[25] Zhang, L., Meng, Q., 2019. Probabilistic ship domain with applications to ship collision risk assessment. *Ocean Engineering*, 186, 106130. https://doi.org/10.1016/j.oceaneng.2019.106130

[26] Im, N., Luong, T. N., 2019. Potential risk ship domain as a danger criterion for real-time ship collision risk evaluation. *Ocean Engineering*, 194, 106610. https://doi.org/10.1016/j.oceaneng.2019.106610

[27] Yang, L., Liu, J., Liu, Z., Luo, W., 2023. Grounding risk quantification in channel using the empirical ship domain. *Ocean Engineering*, 286, 115672. https://doi.org/10.1016/j.oceaneng.2023.115672

[28] Zhang, M., Zhang, D., Fu, S., Yan, X., Goncharov, V., 2017. Safety distance modeling for ship escort operations in Arctic ice-covered waters. *Ocean Engineering*, 146, 202-216. https://doi.org/10.1016/j.oceaneng.2017.09.053

[29] Xu, S., Kim, E., 2025. A Bayesian network model for estimating the combined risk in Northeast Passage escort operations. *Ocean Engineering*, 316, 119932. https://doi.org/10.1016/j.oceaneng.2024.119932

[30] Xu, S., Kim, E., 2023. Hybrid causal logic model for estimating the probability of an icebreaker–ship collision in an ice channel during an escort operation along the Northeast Passage. *Ocean Engineering*, 284, 115264. https://doi.org/10.1016/j.oceaneng.2023.115264

[31] Liu, D., Zheng, Z., Liu, Z., 2024. Research on dynamic quaternion ship domain model in open water based on AIS data and navigator state. *Journal of Marine Science and Engineering*, 12(3), 516. https://doi.org/10.3390/jmse12030516

[32] Li, M., Mou, J., Chen, P., Chen, L., Van Gelder, P. H. A. J. M., 2023. Real-time collision risk based safety management for vessel traffic in busy ports and waterways. *Ocean & Coastal Management*, 234, 106471. https://doi.org/10.1016/j.ocecoaman.2022.106471

[33] Qu, X., Meng, Q., Suyi, L., 2011. Ship collision risk assessment for the Singapore Strait. *Accident Analysis and Prevention*, 43(6), 2030-2036. https://doi.org/10.1016/j.aap.2011.05.022

[34] Yuan, X., Zhang, D., Zhang, J., Wan, C., Fan, L., 2023. A two-stage collision avoidance path planning approach for inland ferries under dynamic channel crossing risk conditions. *Ocean & Coastal Management*, 242, 106692. https://doi.org/10.1016/j.ocecoaman.2023.106692

[35] Gao, J., Zhang, Y., 2024. Ship collision avoidance decision-making research in coastal waters considering uncertainty of target ships. *Brodogradnja*, 75(2), 75203. https://doi.org/10.21278/brod75203

[36] Zarzycki, F., Gil, M., Montewka, J., Szłapczyński, R., Szłapczyńska, J., 2025. Declarative ship arenas under favourable conditions. *Ocean Engineering*, 316, 119927. https://doi.org/10.1016/j.oceaneng.2024.119927

[37] Liu, K., Xin, X., Ma, J., Zhang, J., Yu, Q., 2019. Sensitivity analysis of ship traffic in restricted two-way waterways considering the impact of LNG carriers. *Ocean Engineering*, 192, 106556. https://doi.org/10.1016/j.oceaneng.2019.106556

[38] Jeong, B., Lee, B. S., Zhou, P., Ha, S., 2017. Evaluation of safety exclusion zone for LNG bunkering station on LNG-fuelled ships. *Journal of Marine Engineering & Technology*, 16(3), 121-144. https://doi.org/10.1080/20464177.2017.1295786

[39] Jeong, B., Lee, B. S., Zhou, P., Ha, S. M., 2018. Determination of safety exclusion zone for LNG bunkering at fuel-supplying point. *Ocean Engineering*, 152, 113-129. https://doi.org/10.1016/j.oceaneng.2018.01.066

[40] Jeong, B., Park, S., Ha, S., Lee, J. U., 2020. Safety evaluation on LNG bunkering: To enhance practical establishment of safety zone. *Ocean Engineering*, 216, 107804. https://doi.org/10.1016/j.oceaneng.2020.107804

[41] Duong, P. A., Ryu, B. R., Jung, J., Kang, H., 2023. Comparative analysis on vapor cloud dispersion between LNG/liquid NH3 leakage on the ship to ship bunkering for establishing safety zones. *Journal of Loss Prevention in the Process Industries*, 85, 105167. https://doi.org/10.1016/j.jlp.2023.105167

[42] Zhou, C., Yang, Z., Chen, G., Li, X., 2024. Optimizing hydrogen refueling station layout based on consequences of leakage and explosion accidents. *International Journal of Hydrogen Energy*, 54, 817-836. https://doi.org/10.1016/j.ijhydene.2023.09.210

[43] Jiao, J., Zhao, M., Jia, G., Ding, S., 2024. SPH simulation of two side-by-side LNG ships' motions coupled with tank sloshing in regular waves. *Ocean Engineering*, 297, 117022. https://doi.org/10.1016/j.oceaneng.2024.117022

[44] Xie, C., Huang, L., Wang, R., Deng, J., Shu, Y., Jiang, D., 2022. Research on quantitative risk assessment of fuel leak of LNG-fuelled ship during lock transition process. *Reliability Engineering & System Safety*, 221, 108368. https://doi.org/10.1016/j.ress.2022.108368

[45] Deng, Z., Bai, M., Qi, M., Tian, Y., Qu, H., Liu, Y., 2024. Inherent safety assessment of on-board methanol reforming hydrogen production fuel cell system considering jet fire and vapor cloud explosion. *International Journal of Hydrogen Energy*, 50, 1047-1061. https://doi.org/10.1016/j.ijhydene.2023.08.257

[46] Park, S., Jeong, B., Yoon, J. Y., Kee, J., 2018. A study on factors affecting the safety zone in ship-to-ship LNG bunkering. *Ships and Offshore Structures*, 13(1), 312-321. https://doi.org/10.1080/17445302.2018.1461055

[47] Sun, B., Guo, K., Pareek, V. K., 2014. Computational fluid dynamics simulation of LNG pool fire radiation for hazard analysis. *Journal of Loss Prevention in the Process Industries*, 29, 92-102. https://doi.org/10.1016/j.jlp.2014.02.003

[48] Park, S. I., Paik, J. K., 2022. A hybrid method for the safety zone design in truck-to-ship LNG bunkering. *Ocean Engineering*, 243, 110200. https://doi.org/10.1016/j.oceaneng.2021.110200

[49] Zhang, W., Yan, X., Zhang, D., Zhang, J., 2019. Evaluating the probability of power loss in ship electric propulsion systems based on Bayesian belief networks. *Marine Technology Society Journal*, 53(3), 63-79. https://doi.org/10.4031/MTSJ.53.3.6

[50] Wu, B., Tang, Y., Yan, X., Soares, C. G., 2021. Bayesian Network modelling for safety management of electric vehicles transported in RoPax ships. *Reliability Engineering & System Safety*, 209, 107466. https://doi.org/10.1016/j.ress.2021.107466

[51] Huang, P., Wang, Q., Li, K., Ping, P., Sun, J., 2015. The combustion behavior of large scale lithium titanate battery. *Scientific reports*, 5(1), 7788. https://doi.org/10.1038/srep07788

[52] Wang, Q., Huang, P., Ping, P., Du, Y., Li, K., Sun, J., 2017. Combustion behavior of lithium iron phosphate battery induced by external heat radiation. *Journal of Loss Prevention in the Process Industries*, 49, 961-969. https://doi.org/10.1016/j.jlp.2016.12.002

[53] Qin, P., Sun, J., Wang, Q., 2021. A new method to explore thermal and venting behavior of lithium-ion battery thermal runaway. *Journal of power sources*, 486, 229357. https://doi.org/10.1016/j.jpowsour.2020.229357

[54] Fujii, Y., Shiobara, R., 1971. The analysis of traffic accidents. *The Journal of Navigation*, 24(4), 534-543. https://doi.org/10.1017/S0373463300022372

[55] Yan, X., Wang, K., Yuan, Y., Jiang, X., Negenborn, R. R., 2018. Energy-efficient shipping: An application of big data analysis for optimizing engine speed of inland ships considering multiple environmental factors. *Ocean Engineering*, 169, 457-468. https://doi.org/10.1016/j.oceaneng.2018.08.050

[56] Fu, Y., Lu, S., Li, K., Liu, C., Cheng, X., Zhang, H., 2015. An experimental study on burning behaviors of 18650 lithium ion batteries using a cone calorimeter. *Journal of Power Sources*, 273, 216-222. https://doi.org/10.1016/j.jpowsour.2014.09.039

[57] Wang, Y., Lu, X., Zhang, Y., Liu, L., 2024. Hazard comparison of thermal runaway of electric marine battery cabinet under different trigger modes. *International Journal of Heat and Mass Transfer*, 228, 125689. https://doi.org/10.1016/j.ijheatmasstransfer.2024.125689

[58] Fan, H., Zhang, H., Xu, J., 2013. Analysis of pool fire hazard distance for LNG bunkering barges. *Shipbuilding of China*, 54(4), 186-195.

[59] Raj, P. K., 2007. LNG fires: A review of experimental results, models and hazard prediction challenges. *Journal of hazardous materials*, 140(3), 444-464. https://doi.org/10.1016/j.jhazmat.2006.10.029

[60] Farrington, M. D., 2001. Safety of lithium batteries in transportation. *Journal of power sources*, 96(1), 260-265. https://doi.org/10.1016/S0378-7753(01)00565-1

[61] Chen, Q., Liu, C., Yi, W., 2019. A method for establishing the length of moving safety zone around LNG carrier sailing in Yangtze River downstream. *Proceedings of the Twenty-ninth (2019) International Ocean and Polar Engineering Conference*, 16-21 June, Honolulu, Hawaii, USA.

[62] Weng, Y., Sun, H., 2014. Simulation of traffic in two-way navigable channels. *Navigation of China*, 37(1), 103-130.

[63] P.H. Thomas., 1963. The size of flames from natural fires. *Proceedings of the Combustion Institute*, 9(1), 844-859. https://doi.org/10.1016/S0082-0784(63)80091-0

[64] Moorhouse, J., 1982. Scaling criteria for pool fires derived from large-scale experiments. *Institution of Chemical Engineers Symposium Series*, 71, 165-179.

[65] Ji, J., Ge, F., Qiu, T., 2021. Experimental and theoretical research on flame emissivity and radiative heat flux from heptane pool fires. *Proceedings of the Combustion Institute*, 38(3), 4877-4885. https://doi.org/10.1016/j.proci.2020.05.052

[66] Palacios, A., Muñoz, M., Darbra, R. M., Casal, J., 2012. Thermal radiation from vertical jet fires. *Fire safety journal*, 51, 93-101. https://doi.org/10.1016/j.firesaf.2012.03.006

[67] Lowesmith, B. J., Hankinson, G., Acton, M. R., Chamberlain, G., 2007. An overview of the nature of hydrocarbon jet fire hazards in the oil and gas industry and a simplified approach to assessing the hazards. *Process safety and environmental protection*, 85(3), 207-220. https://doi.org/10.1205/psep06038